Dispersion forces and equilibrium distance between deposited rough films in contact

I. A. Soldatenkov and F. I. Stepanov
Ishlinsky Institute for Problems in Mechanics, Russian Academy of Sciences, prospect Vernadskogo, 101-1, 119526 Moscow, Russia

V. B. Svetovoy*
Frumkin Institute of Physical Chemistry and Electrochemistry, Russian Academy of Sciences, Leninsky prospect 31 bld. 4, 119071 Moscow, Russia

(Received 6 September 2021; revised 23 January 2022; accepted 26 January 2022; published 1 February 2022)

The average distance h_0 separating two contacting bodies is a critical parameter for many problems, for example, for control of unwanted stiction in micro/nanoelectromechanical systems. Here this problem is analyzed in relation to precise determination of the dispersion forces in a difficult for measurement range of $5-30$ nm. The unloaded contact between two deposited rough films characterized by a relatively large number of high asperities is considered. The equilibrium distance h_0 can be found from the balance of attractive dispersion forces and repulsive forces acting in the spots of real contact. A simple columnar model associated with AFM images of rough surfaces is used to describe the balance. The numerical analysis, which treats the high asperities as elastoplastic semispheroids, demonstrates that the columnar model describes the contact adequately. It is shown that in contrast with the value of h_0 the adhesion energy between the surfaces is nearly entirely defined by the dispersion interaction, but the effects of contact interaction and plastic deformations can be neglected. This property is proposed to use for more precise determination of the equilibrium distance.

DOI: 10.1103/PhysRevB.105.075401

I. INTRODUCTION

Dispersion forces (DFs) acting between uncharged bodies originate from quantum fluctuations of electromagnetic field. At distances of the order of 1 nm they are called van der Waals (vdW) forces, but at larger separations, when the retardation of the electromagnetic signal becomes important, they are called Casimir [1] (or retarded vdW) forces. Since the physical origin of the forces is the same, a general name DFs can be used. Lifshitz and co-workers [2,3] proposed a macroscopic theory of the DFs, which expresses the forces via the dielectric functions of interacting materials. The last two decades have seen significant progress in understanding of the forces [4,5]. The forces have been measured at distances of the order of 100 nm with a high precision of 1% in a series of experiments [6–10], which demonstrated a good agreement with the predictions of the Lifshitz theory. The dependence on the dielectric functions of different materials has been checked in special experiments [11–15]. Measurement of the forces at separations shorter than 50 nm are sparse and not very precise [16–18] due to pull-in instability of the elastic suspension systems used for measurement. Recently a method of adhered cantilever [19,20] has been proposed to measure the forces at shorter separations, which does not suffer from the pull-in instability.

The problem that is considered in this paper stems from the precise measurements of the Casimir forces but has much broader interest. An important parameter that has to be measured together with the force is the distance of minimal approach h_0 between the surfaces used for the force measurement [6–10]. This parameter is responsible for the main part of the experimental uncertainty and is typically determined from the electrostatic calibration with a precision of 1 nm. In most cases h_0 is determined at distances far away from the physical contact.

In the method of adhered cantilever [20] proposed recently (see the scheme in Fig. 1) the adhered end is in physical contact with the substrate where the separation h_0 between the contacting surfaces is also a critical parameter. The better we know the separation h_0 the more precise we can determine the force from the shape of the cantilever. One can also look at the problem from a different angle. When two rough plates are in contact, the adhesion energy Γ between them at certain conditions is completely defined by the DFs [21] at the average separation h_0. Therefore, we can get the information on the dispersion interaction by measuring Γ and h_0. Experimentally it is simpler to find Γ than determine the shape of the cantilever with a precision of 1 nm. However, theoretically it is not that straightforward to find the function $\Gamma(h_0)$ because roughness is an essential part of the problem.

It is worth to note that the contact of rough surfaces occurs on the highest asperities. In the places of direct contact rather strong forces are involved, which operate at distances $\lesssim 1$ nm, which are close to the molecular scale. On the other hand, the asperities, which are not in direct contact, interact with weaker DFs, but the area of this noncontact interaction is much larger. Thus, measuring the forces with the adhered cantilever we probe the transition between the discrete molecular and continuous scales. Practically all the existing measurements of the DFs have been performed in the sphere-plate geometry. Only in three papers [22–24] the forces were measured between

*Corresponding author: v.svetovoy@phyche.ac.ru

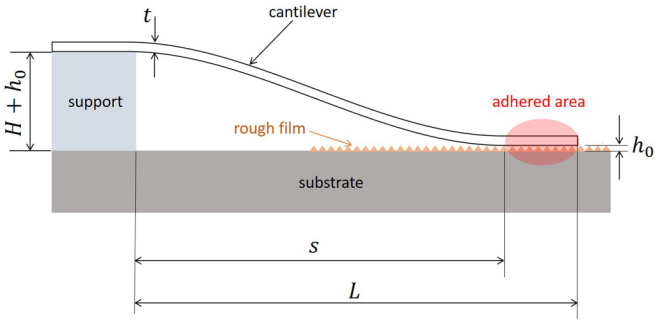

FIG. 1. Scheme of the adhered cantilever. The left end is firmly fixed at the height H in comparison with the right end. The latter is adhered to the substrate with a rough film on top of it. The equilibrium distance between the cantilever and rough surface is h_0. The parameters s and L are the unadhered length and total length of the cantilever, respectively.

parallel plates. The method of adhered cantilever is naturally designed in such a way that the forces are measured between practically parallel surfaces.

The distance between solids in contact has a fundamental significance for the interaction between bodies including capillary, dispersion, and other surface forces. This distance defines the adhesion energy between surfaces that controls, for example, such a phenomenon as stiction in microsystems [25–27]. Besides, it is closely related to the problems of contact resistivity [28,29], sealing and lubrication [30], heat transfer [31–33], contact mechanics [34,35]. Determination of the distance between contacting surfaces is one of the tasks of the contact mechanics problem.

In a seminal paper by Greenwood and Williamson [36], the rough topography was described as an ensemble of asperities with the same curvature radius of summits and with a random height that follows the normal distribution. The influence of roughness on the equilibrium distance between contacting surfaces has been analyzed in this single-scale asperity model. The effect of adhesion on the contact of rough surfaces has been taken into account by Fuller and Tabor [37], who demonstrated that adhesion becomes important at small loads.

The single-scale asperity model has been generalized to the multiscale case including fractal nature of the surface topography [34,38–43]. It was demonstrated that asperities separated by the in-plain distances smaller than the correlation length can influence each other providing the deviations from the single-scale asperity model. The question of mutual influence of the asperities was also investigated for deterministic multiscale contact [44], where it was found that for a sufficiently large distance between the asperities their mutual influence can be neglected.

The theories of rough contact usually assume elastic contact between solids and a Gaussian height distribution of the asperities (see, however, [45]). For the problem considered in this paper both of these assumptions are broken and we cannot use directly the developed theories for the following reasons.

First, the problem is solved for thin metallic films deposited on a substrate at room temperature by thermal evaporation or magnetron sputtering. Such surfaces are typical for microfabricated devices. It was noted that thermally evaporated thin films of oligomer [46] and gold [47] demonstrate excessive number of high asperities in comparison with the normal distribution. Very recent analysis [48] of different materials (W, Pt, Cu, SiO_2) magnetron sputtered on Si substrate at room temperature demonstrated that the excessive number of high asperities is observed for all the investigated materials. Because the films deposited on hot substrates follow the Gaussian roughness distribution, one can expect that the large number of high asperities is generated due to the nonequilibrium deposition conditions. To feel the magnitude of the effect let us compare the number of peaks with the height $h > 5w$ for 200-nm-thick Pt film that has the root-mean-square (rms) roughness $w = 1.0$ nm. The area investigated with an atomic force microscope (AFM) was $20 \times 20\ \mu\text{m}^2$ and the correlation length was found to be $\xi = 20$ nm (typical size of the features on the surface is 2ξ). The number of high peaks determined from the AFM image was about 800, but the normal distribution predicts less than one high peak (≈ 0.3) in this area.

Second, the experiments measuring the Casimir forces demonstrate that the equilibrium distance between the bodies is considerably larger than the rms roughness [49] and for gold this distance is typically as large as $h_0 = (4-6)w$. At the separations $h_0 \sim 10$ nm the Casimir pressure between the surfaces is $P_C(h_0) = 10^4 - 10^5$ Pa. If the lateral size of the asperity is 2ξ and the size of the nominal area of contact is $\mathcal{L}$, then the local pressure on the highest asperity will be $P_{loc} = P_C(\mathcal{L}/2\xi)^2$. For $\mathcal{L} = 100\ \mu$m and $\xi = 20$ nm, one finds $P_{loc} = 10^{11} - 10^{12}$ Pa that exceeds the flow stress for any metal. This estimation is conservative and we can expect that the number of high asperities deformed plastically will be much larger than just one.

Also it is worth to note that small elastic deformations of the high asperities are balanced by the attractive interaction between bodies that can be due to capillary, electrostatic or other surface forces, but in this paper we consider only the DFs, which cannot be excluded by any special preparation of the surfaces. This interaction results in a rather weak adhesion energy between the surfaces $\lesssim 100\ \mu\text{J/m}^2$ that can be compared with the adhesion $\gtrsim 100\ \text{mJ/m}^2$ [50] typically considered for rough contact. In spite of the weak adhesion the DFs have to be carefully controlled in micro/nanoelectromechanical systems (MEMS/NEMS) because they can lead to unwanted stiction of separate elements during fabrication or operation [25–27].

The adhered cantilever shown in Fig. 1 has been used as a test system [26,51] for analysis of the weak adhesion between rough surfaces. The adhesion energy per unit area Γ can be expressed via the unadhered length s [52–54]. The value of Γ has been determined for a number of materials but only one attempt has been made to relate its value to the DFs acting in the gap between the contacting surfaces [55]. It has been concluded that the main contribution to the adhesion energy comes from the dispersion interaction acting across the average gap separating the contacting surfaces.

This paper presents a full version of the Letter [21] in which a relation between the adhesion energy Γ and the distance upon contact h_0 has been deduced. The most important conclusion was that for a couple of interacting material the function $\Gamma(h_0)$ does not depend on the parameters of

short-distance interaction and can be considered as universal. This function can be found within the Lifshtz theory. On the contrary, the equilibrium distance is sensitive to the parameters of the short-distance interaction. In this paper we provide the details of the analytical model that allows calculation of the average separation gap between a flat and rough surfaces based on the roughness statistics of asperities of the deposited films and plastic deformation of high asperities. This information is used to calculate the adhesion energy between the surfaces in contact. We demonstrate numerically that the simple columnar model of asperities is adequate to the real situation.

II. THEORY

A rough adhesive contact is modelled on the basis of a single-asperity contact. The solutions of this problem used the concept of surface (adhesion) energy were pioneered by Johnson, Kendall, and Roberts [56] and Derjaguin, Muller, and Toporov [57] who applied different approaches. A strict formulation of the contact problem in the presence of intermolecular interactions assumes the existence of a certain gap between the contacting bodies. The size of this gap depends on the deformation of the bodies and has to ensure the equivalence of the deformation and intermolecular forces at the contact (Derjaguin's self-consistent approach [58]). For the first time the contact problem based on the self-consistent approach was considered for a spherical Hertz contact in the presence of intermolecular interactions described by the Lennard-Jones potential [58]. This approach was developed further in many studies (see, for example, [59–61]).

A. Formulation of the problem

Let us consider two rough plates getting into the mechanical contact. A special analysis provided by Greenwood and Trapp [62] demonstrated that this problem can be simplified. One can consider instead a compliant rough plate with the combined roughness, which is the sum of the two topographies, and a rigid flat plate. The validity of this statement is based on a simple fact that the asperities on two surfaces are misaligned. The plastic deformations of the combined rough plate are defined by the softest material. As an example close to this effective configuration we consider the interaction of a smooth Si plate with an rms roughness of $0.2-0.3$ nm (cantilever) and a Si wafer with the deposited thin layer of a metal with larger rms roughness.

Figure 2 shows the cross-section profile of a Pt film magnetron sputtered on Si substrate [48]. The reference plane is taken at the average height of the film. When the flat plate approaches the rough one the bodies contact on the highest asperities, which are deformed elastically and plastically and some equilibrium distance h_0 is established as a balance of the attractive DFs and repulsive forces in the places of contact. The elastic deformations are much smaller than the plastic ones, but the energy of the elastic deformations is collected in the bulk of the bodies while the energy needed to produce plastic deformations dissipates.

The attractive force between the plates varies locally due to the roughness. According to the Lifshitz theory the force has to diverge in the places of direct contact. Indeed, it is not possible physically and the local separation stays finite due to short-range repulsion of electron clouds. To this end we introduce at short distances the Lennard-Jones intermolecular potential

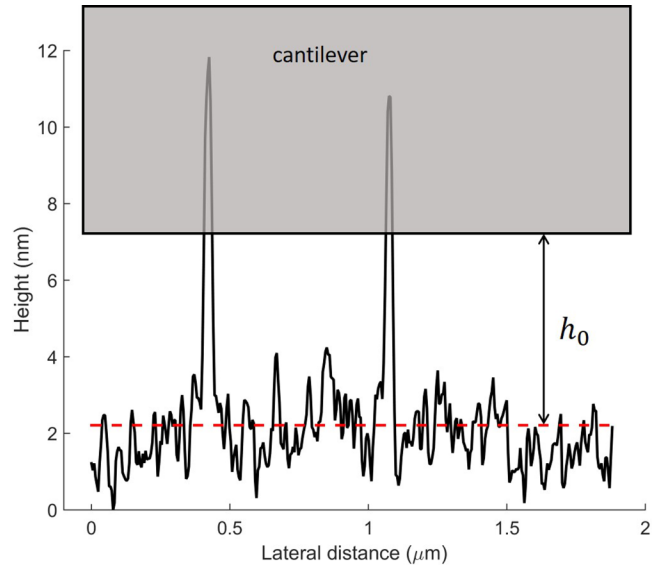

FIG. 2. The profile of a 200-nm-thick Pt film that is in contact with a flat surface of the cantilever ($w = 1.0$ nm, $\xi = 20.0$ nm). The average position of the rough surface is shown by the red dashed line. Only high peaks are in direct contact with the rigid surface of the cantilever. These peaks are deformed elastically and plastically.

$$u_{LJ}(r) = -4\epsilon_0[(\sigma/r)^6 - (\sigma/r)^{12}], \tag{1}$$

where ϵ_0 and σ are the parameters specific for each pair of molecules and r is the distance between the molecules. The pressure between parallel plates separated by the distance h [63] calculated with the use of the potential (1) is

$$P_{LJ}(h) = -\frac{A_H}{6\pi h^3}\left[1 - \left(\frac{h_c}{h}\right)^6\right], \tag{2}$$

where A_H is the Hamaker constant. Both parameters A_H and h_c are related to the original parameters ϵ_0 and σ but for A_H this relation has no special meaning because the attractive vdW forces [first terms in (1) and (2)] are not additive. On the other hand, the molecular size σ does not change significantly when the molecules are arranged in a solid and the relation $h_c = (2/15)^{1/6}\sigma$ has sense. We can conclude that h_c has the meaning of the equilibrium distance between parallel plates without application of an external load.

The prefactor in Eq. (2) describes the vdW force and is the short distance asymptotic of the DF. At larger separations one has to take into account the effect of retardation and at arbitrary distances the prefactor has to be changed by the Lifshitz formula for the DFs. This procedure is justified because the second term in (2) can be neglected already at $h \sim 1$ nm since typical value for the equilibrium distance is $h_c = 0.2 - 0.3$ nm [64]. After these explanations one can generalize the DF to include the short distance repulsion. The

pressure between two parallel plates can be written as

$$P(h) = P_{\mathrm{Lif}}(h)[1 - (h_c/h)^6]. \tag{3}$$

The function $P_{\mathrm{Lif}}(h)$ has to be calculated using the Lifshitz theory [3], where one can neglect the thermal fluctuations since in the range of distances important for this study ($h \sim 10$ nm) the quantum fluctuations dominate and the thermal effect is very small. The calculation procedure is nontrivial but have been described in many papers [3,4] and textbooks [65] and will not be repeated here. It includes as inputs the dielectric functions $\varepsilon_{1,2}(\omega)$ of interacting materials in a wide range of frequencies ω.

The problem that will be solved in this paper consists of two parts. First, we determine the equilibrium distance h_0 between the flat rigid plate and the rough plate that can be deformed plastically and elastically. Second, for a given distance h_0 we determine the adhesion energy per unit area Γ between these two plates. Both values can be directly measured experimentally in the proposed experiment [20] and compared with the theoretical prediction.

B. Columnar model of roughness

We consider first the simplest model of the rough surface, which will highlight the most important steps in determination of the equilibrium distance h_0. In this model it is assumed that the rough surface consists of columns with equal cross sections $A_\xi = 4\xi^2$ and random height h_i, where the index i enumerates the columns. The height of the columns can be positive or negative with respect to the reference plane. In this simplified model the tops of the columns are considered flat. When the contact pressure is applied to a column, it is deformed plastically provided that the pressure is larger than the stress needed for plastic deformation P_f (flow stress). Despite its simplicity this model seems to be adequate to the considered problem of crumpling high and rare peaks.

It is worth noting that the columns loaded in this way are also deformed elastically, but the elastic deformations are small in comparison with the plastic ones. Really, if the ith column is stressed homogeneously, it is deformed as $\delta h = (P_f/E_r)h_i$, where E_r is the Young modulus of the rough plate. On one hand, this value is small in comparison with h_i because for all metals $P_f \ll E_r$. On the other hand, the elastic deformation is small in absolute terms because for $h_i \sim 10$ nm and for the ratio $P_f/E \sim 10^{-3}$ one has $\delta h \sim 0.1$ Å that is equal to the vertical resolution of AFM and is much smaller than the plastic deformations.

Following the Derjaguin self-consistent approach [58] we assume the existence of a certain gap h_{0c} between the contacting columns and the flat plate (Fig. 3). The size of this gap has to ensure the balance between the flow stress P_f and intermolecular forces, so that according to Eq. (3) one finds the relation

$$P_f = P(h_{0c}), \tag{4}$$

which is valid for any column in contact. The force acting on the contacting columns is repulsive and for this reason $h_{0c} < h_c$. The force between the flat plate and a column, which is not in contact, is defined by the long-distance intermolecular forces in correspondence with Eq. (3).

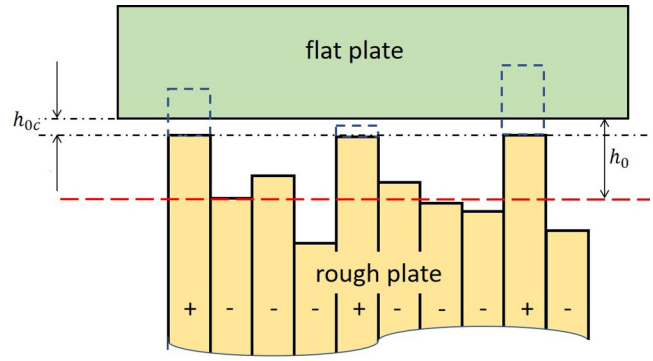

FIG. 3. Columnar model for rough films. The red dashed line shows the average plane of the rough surface (reference plane). The rough profile is shown after plastic deformation of some columns whose original position is indicated by the blue dashed lines. The columns deformed plastically are marked by the sign "+" while the columns which are not deformed are marked by the sign "–". The distance h_{0c} is the distance of closest approach (contact gap).

Let $A_{\mathrm{nom}} = \mathcal{L}^2$ be the nominal area of contact. The total number of columns is $N_{\mathrm{tot}} = A_{\mathrm{nom}}/A_\xi = (\mathcal{L}/2\xi)^2$. When the bodies approach each other some high peaks are deformed plastically. In the simple columnar model we take into account only the reduction of the column heights but do not consider the change of their area. The latter effect will be accounted numerically in an advanced version of the roughness model (see Sec. III). At the distance between the bodies h the relative area of contact $R(h)$ is

$$R(h) = \int_{h_p}^{\infty} dz f(z), \quad h_p = h - h_{0c}, \tag{5}$$

where $f(z)$ is the density distribution function of column heights.

When the plates approach or retreat, the forces between them are different because plastic deformations are not recovered. For our purposes it is sufficient to know only the force during the retraction since it allows us to deduce the force balance equation and calculate the adhesion energy. When the plates are in contact at the equilibrium position, the distance between them is $h = h_0$. The height of the contacting columns in this position is $h_{0p} = h_0 - h_{0c}$ and the relative area of contact is $R(h_0)$. When the flat plate retreats the height and area of these columns do not change and the force from them (marked with "+" in Fig. 3) is

$$F_+(h) = A_{\mathrm{nom}} P(h - h_{0p}) R(h_0).$$

Contrarily, the force from the columns that never have been in contact (marked with "–" in Fig. 3) is

$$F_-(h) = A_{\mathrm{nom}} \int_{-\infty}^{h_{0p}} dz f(z) P(h - z).$$

The total force per unit area at the distance h will be

$$P_{\mathrm{tot}}(h) = \int_{-\infty}^{h_{0p}} dz f(z) P(h - z) + P(h - h_{0p}) R(h_0). \tag{6}$$

At $h = h_0$ the plates are in equilibrium where the total force has to be zero. In this point $P(h_0 - h_{0p}) = P(h_{0c})$ and

according to (4) it is equal to P_f. Then one finds from Eq. (6)

$$\int_{-\infty}^{h_{0p}} dz f(z) P(h_0 - z) = -P_f R(h_0). \quad (7)$$

This equation describes the balance of the forces and allows determination of the unknown equilibrium distance h_0. The left side presents the attractive forces acting between the plates, while the right side describes the short-distance repulsion.

If the force between the plates is known, the adhesion energy can be found as the work needed to remove one plate from the equilibrium distance h_0 to infinity. This work is

$$\Gamma(h_0) = -\int_{h_0}^{\infty} dh P_{\rm tot}(h)$$
$$= -\int_{-\infty}^{h_{0p}} dz f(z) W(h_0 - z) - R(h_0) W(h_{0c}). \quad (8)$$

Here $W(h)$ is the dispersion energy (per unit area) between two flat plates separated by the distance h defined as

$$W(h) = \int_h^{\infty} dx P(x). \quad (9)$$

The relation (8) defines the adhesion energy Γ. The Eqs. (7) and (8) solve the problem in the frame of the simple columnar model.

C. Equilibrium distance

From an AFM image of the rough surface one can determine the density distribution function of separate pixels $f_p(z)$ but not the distribution function $f(z)$ of asperities that enters Eq. (7). However, for the simple columnar model this difference is not important. It is obvious for the left-hand side of Eq. (7) because the columns do not contact with the flat plate and as an elementary column one can take an AFM pixel. This is true also for the right-hand side because in the simple model it is assumed that the cross section of the deformed columns does not change and the area of real contact can be calculated as the sum over all the pixels, which are deformed by the flat plate.

The function $f_p(z)$ extracted from any AFM image is the number of pixels with the heights from z to $z + \Delta z$ relative to the total number of pixels and to the interval Δz. For the 200-nm-thick Pt film magnetron sputtered and Au film thermally evaporated on Si substrate the distribution functions are shown in Figs. 4(a) and 4(b), respectively. One can clearly see that the number of high pixels in both cases is considerably larger than that predicted by the normal distribution (dashed curve).

The force $P_{\rm Lif}(h)$ is calculated following the Lifshitz theory [3,65]. To find this force, one has to know the dielectric functions of the interacting materials at imaginary frequencies $\varepsilon(i\zeta)$. With the help of the Kramers-Kronig relation $\varepsilon(i\zeta)$ can be expressed via the dielectric function at real frequencies $\varepsilon(\omega)$, which is directly measurable. For Si crystal the dielectric function is well documented and it was calculated using the handbook [66] optical data. For gold $\varepsilon_{Au}(i\zeta)$ was extracted from the spectral ellipsometry data [67] collected from the thermally evaporated films. As a representative example, sample 3 in [67] has been chosen. For Pt the corresponding

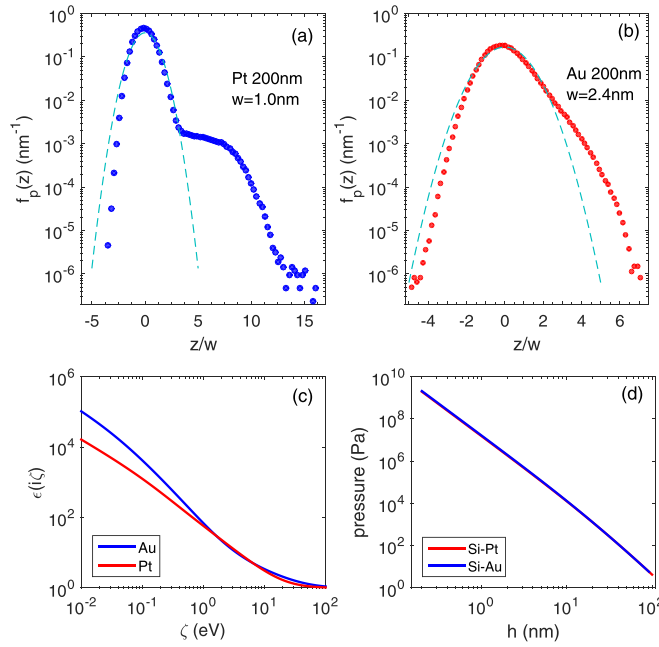

FIG. 4. (a) The density distribution function for Pt film extracted from the AFM data [48]. The dashed curve corresponds to the normal distribution with the same rms roughness. (b) The same as (a) but for Au film thermally evaporated. (c) The dielectric functions of Pt and Au at imaginary frequencies. (d) The attractive forces $P_{\rm Lif}(h)$ calculated for Si-Pt and Si-Au systems. The forces for these two systems nearly coincide (see text).

dielectric function $\varepsilon_{Pt}(i\zeta)$ was taken from [68] where the film was magnetron sputtered on Si substrate and the data were collected from the reflectance spectrum. The dielectric functions of metals are shown in Fig. 4(c). The imaginary frequencies that give the main contribution to the force $P_{\rm Lif}(h)$ are of the order of the characteristic frequency $\zeta_{ch} = c/2h$ (it is not true for real frequencies). For h in the interval $1 - 100$ nm the frequency ζ_{ch} varies in the range $1 - 100$ eV. As one can see from the figure in this range the dielectric functions of Pt and Au differ only slightly. For this reason one can expect that the forces for Si-Au and Si-Pt will be close to each other. It is really the case as one can see in Fig. 4(d). The maximum difference of about 10% is realized at $h = 0.2$ nm.

To take into account the short-distance repulsion in Eq. (3) one has to know the parameter h_c. As we already mentioned it is related to the parameter σ in the Lennard-Jones potential as $h_c = (2/15)^{1/6}\sigma$. For interaction of two equivalent molecules the values of σ used often in molecular dynamics simulations are the following $\sigma_{Si} = 0.392$ nm [69], $\sigma_{Au} = 0.293$ nm [69], and $\sigma_{Pt} = 0.247$ nm [70]. When two different molecules 1 and 2 interact we use the Loretz mixing rule $\sigma = (\sigma_1 + \sigma_2)/2$ used in molecular dynamics. Thus, we find for Si-Au interaction $h_c = 0.245$ nm and for Si-Pt interaction $h_c = 0.228$ nm.

An additional parameter that has to be known is the flow stress P_f. This parameter can depend on many factors; for bulk materials a range of values is usually provided in dependence of the material preparation method, but for the deposited thin films additional uncertainties appear related to the film nanostructure [71]. For Au the stress-strain curves were directly measured [72–75] for nanostructured samples.

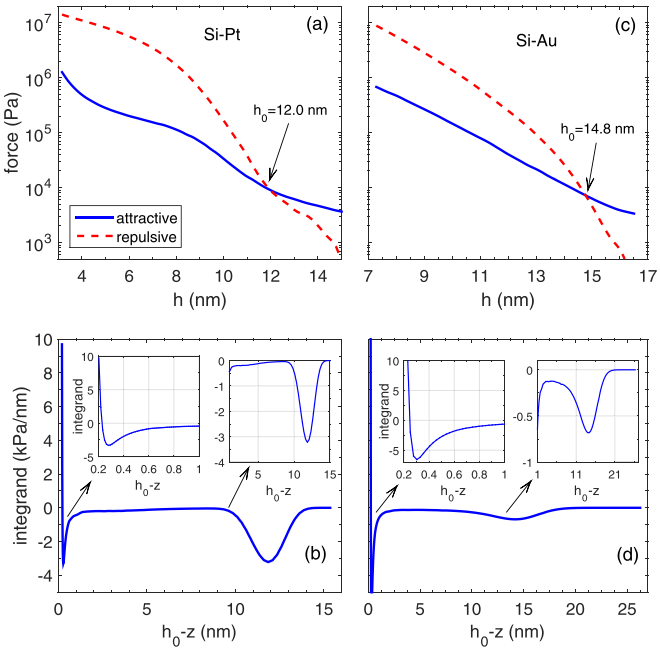

FIG. 5. Determination of the equilibrium distance h_0. (a) Attractive (solid) and repulsive (dashed) forces between flat Si and rough Pt plates calculated as the left and right sides of Eq. (7), respectively. The cross point gives the equilibrium distance. (b) The integrand for the attractive force as a function of asperities height z. The insets show the short and long distance behavior. (c) and (d) are the same as (a) and (b) but for Si-Au interaction.

For single crystals the experiments demonstrate significant increase of the flow stress with the size decrease. For the deposited films the grains can be considered as single crystals and roughly the flow stress for Au can be estimated as $P_f \approx 1$ GPa. For Pt single crystal the molecular dynamic simulations [76] give $P_f \approx 1.8$ GPa. The direct measurement [77] for nanostructured samples gave close but somewhat smaller value. However, uncertainties in P_f are too large to choose any specific value for a given material without knowing details of the nanostucture.

Considering the left and right sides of Eq. (7) as independent functions of the distance h we can find the solution as a cross-point at $h = h_0$. Figure 5(a) shows the attractive (solid curve) and repulsive (dashed curve) forces, respectively. The cross-point corresponds to the equilibrium distance h_0, which we are looking for. It has to be stressed that although the rms roughness of Pt film is $w = 1.0$ nm the value of $h_0 = 12.0$ nm is significantly larger. In panel (c) the same is shown for Au film with the rms roughness $w = 2.4$ nm and $h_0 = 14.8$ nm. As follows from Fig. 4(d) the forces Si-Pt and Si-Au between flat plates are very close to each other. The difference between the attractive (and repulsive) forces in Figs. 5(a) and 5(c) are explained by the different character of roughness. Figure 5(b) demonstrates the integrand in the attractive force at $h = h_0$ (for Pt). One can see (see also the insets) that there are two main contributions to the force. The first contribution originates from the non-touching high peaks with heights in a narrow range $h_0 - h_s < z < h_{0p}$, which approach to the flat plate closer than h_s. Conventionally we choose for h_s the value $h_s = 1$ nm, but the results are not very sensitive to h_s in the nanometer range. The second one originates from the typical asperities, for which the local distance between the bodies is of the order of h_0. These contributions are $P_{a1} = 0.84$ kPa and $P_{a2} = 8.29$ kPa so that the total attractive pressure is $P_a = P_{a1} + P_{a2} = 9.13$ kPa. For Si-Au interaction these values are $P_{a1} = 1.73$ kPa and $P_{a2} = 5.45$ kPa. For gold the second contribution is smaller but still dominates over the short distance contribution.

It is interesting to compare these results with the case when the roughness is described by the Gaussian distribution with the same rms value. For the normal roughness distribution we have found for Si-Pt interaction the equilibrium distance $h_0 = 3.3$ nm that is considerably smaller than a value of 12.0 nm that takes into account the high peaks. This difference is easy to understand because for the normal distribution the highest peaks are about of $(3-4)w = 3-4$ nm. Indeed for smaller h_0 the equilibrium pressure is much larger: $P_a = 1.29$ MPa and the role of the short-distance interaction is more important: $P_{a1} = 0.52$ MPa. For the case of Si-Au interaction the difference is also significant but less dramatic. For the Gaussian roughness distribution of Au we have found $h_0 = 9.5$ nm, $P_a = 40.8$ kPa, and $P_{a1} = 9.6$ kPa.

D. Adhesion energy

Now let us discuss the adhesion energy Γ. In the first term in Eq. (8) one can separate the contribution of asperities which approach so close to the flat plate that the local distance is in the range $h_{0c} < h_0 - z < h_s$. Combining this contribution with the second term in (8) we introduce a "nearly" contact contribution to Γ:

$$\Gamma_c(h_0^*) = -\int_{h_{0c}}^{h_s} dx f(h_0^* - x) W(x) - W(h_{0c}) R(h_0^*), \quad (10)$$

where a new integration variable $x = h_0^* - z$ has been introduced. The rest is the noncontact contribution

$$\Gamma_{nc}(h_0^*) = -\int_{h_s}^{\infty} dx f(h_0^* - x) W(x). \quad (11)$$

Note that h_0^* in Eqs. (10) and (11) is a variable in contrast with h_0, which is still an equilibrium distance. The argument h_0^* is considered as a variable because P_f is not well-defined parameter and change in P_f will correspond to the change in the equilibrium distance.

If only the DFs and short-range repulsion are acting in the area of direct contact then

$$W(h_{0c}) = -\frac{A_H}{12\pi h_{0c}^2}\left[1 - \frac{1}{4}\left(\frac{h_c}{h_{0c}}\right)^6\right] \quad (12)$$

is the contact energy at $h = h_{0c}$ that is the integral from the force (2) with the opposite sign. From the used optical data the Hamaker constant for Si-Pt system is $A_H = 29.0 \times 10^{-20}$ J and from Eq. (4) one finds $h_{0c} = 0.204$ nm, then the contact energy is $W(h_{0c}) = -94.6$ mJ/m^2. For the Si-Au system it was found, $h_{0c} = 0.225$ nm, $A_H = 31.3 \times 10^{-20}$ J, and $W(h_{0c}) = -95.5$ mJ/m^2. Although for both systems the absolute value of $W(h_{0c})$ is quite large, its contribution to Γ is small because the relative area of real contact $R(h_0)$ is small.

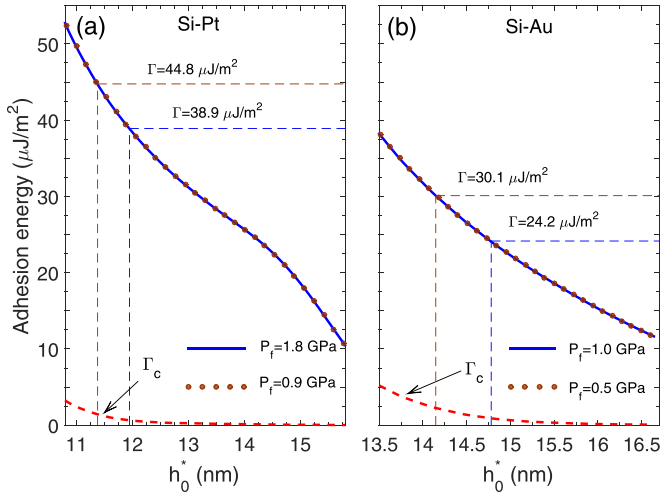

FIG. 6. (a) The adhesion energy as a function of distance h_0^* for Si-Pt system. The blue curve shows the total energy for $P_f = 1.8$ GPa and red dashed curve shows the contact adhesion energy. The curve marked by brown dots corresponds to the total energy for $P_f = 0.9$ GPa. The straight dashed lines indicate the equilibrium positions for both P_f. (b) The same as (a) but for Si-Au system with $P_f = 1.0$ GPa and $P_f = 0.5$ GPa.

Figure 6 shows Γ (solid blue curve) and its contact components Γ_c (dashed red curve) as functions of varied distance h_0^*. At the equilibrium distance $h_0^* = h_0$ the noncontact contribution dominates and we found that the total and contact adhesion energies for Si-Pt are $\Gamma = 38.9\ \mu\text{J/m}^2$ and $\Gamma_c = 0.65\ \mu\text{J/m}^2$ for $P_f = 1.8$ GPa, respectively. For Si-Au system it was found $\Gamma = 24.2\ \mu\text{J/m}^2$ and $\Gamma_c = 0.91\ \mu\text{J/m}^2$ for $P_f = 1.0$ GPa. Note that the contact contribution to Γ is small. For Si-Pt the relative contribution of Γ_c at equilibrium distance $h_0 = 12.0$ nm is 1.7% and for Si-Au at $h_0 = 14.8$ nm it is 3.8%. It is an important property of the adhesion energy that says that the main contribution to Γ comes from pure DFs.

If similar calculations will be performed for Gaussian roughness distribution the adhesion energy will be significantly larger mostly owing to smaller equilibrium distance h_0. For Si-Pt interaction we have found $\Gamma = 1137\ \mu\text{J/m}^2$ and $\Gamma_c = 79\ \mu\text{J/m}^2$. Here the role of the short-distance interaction (Γ_c) is more important in comparison with the actual distribution of roughness but still far from dominating. For Si-Au interaction it was found $\Gamma = 94.3\ \mu\text{J/m}^2$ and $\Gamma_c = 3.9\ \mu\text{J/m}^2$.

One has to stress also the following. The value of Γ can be relatively easily measured with a good precision by the adhered cantilever method, but the experimental determination of the equilibrium distance is more difficult and a typical precision of ± 1 nm is not sufficient for small separations $\sim$10 nm. Knowledge of the function $\Gamma(h_0^*)$ allows precise determination of h_0 via the measured value of Γ. Equation (8) provides this function if all other forces but the DFs are excluded. One would expect a significant uncertainty in Γ due to not well defined flow stress, but it is not the case. The parameter P_f does not appear in $\Gamma(h_0^*)$ explicitly but manifests itself via the value of h_{0c} [see Eq. (4)] and this dependence is weak because of sharp variation of the function $P(h)$ near $h = h_{0c}$. If we reduce P_f twice the function $\Gamma(h_0^*)$ changes negligibly as the curve in Fig. 6 marked with brown dots shows, but the equilibrium distance can change more significantly because P_f enters explicitly in Eq. (7). It means that when P_f varies the function $\Gamma(h_0^*)$ stays practically the same, but the value of $\Gamma = \Gamma(h_0)$ corresponding to the equilibrium situation changes. This dependence can be used in the opposite direction: Using the measured value of $\Gamma = \Gamma(h_0)$ we can determine unknown h_0 with a good precision. For Si-Pt system with $P_f = 0.9$ GPa we have found the equilibrium values $h_0 = 11.2$ nm and $\Gamma = 44.8\ \mu\text{J/m}^2$ and for Si-Au system with $P_f = 0.5$ GPa the corresponding values are $h_0 = 14.1$ nm and $\Gamma = 30.1\ \mu\text{J/m}^2$.

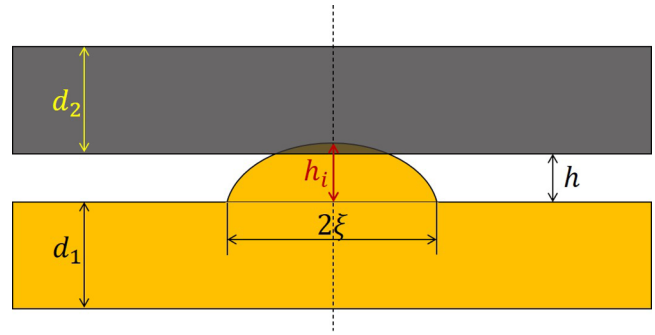

FIG. 7. Schematic presentation (out of scale) of the elastoplastic problem of compression of a semispheroid bump with the height h_i and diameter 2ξ. Both upper and lower substrates have equal thickness $d_1 = d_2 = 50$ nm.

The reason for the weak sensitivity of the function $\Gamma(h_0^*)$ to the value of P_f is also related to a small area of real contact. For example, for Si-Pt the relative area is $R(h_0) = 4.1 \times 10^{-6}$ and in spite of large $W(h_{0c})$ the contact contribution to Γ is small. On the other hand, the small area of real contact is due to excessive number of high peaks in the deposited films in comparison with the normal distribution. Materials with the normal roughness distribution would have much larger area of real contact because the equilibrium distance for these materials will be as small as $(2-3)w$ and much larger number of asperities will be in direct contact. Then the contact contribution to Γ will dominate and the adhesion energy will be significantly larger (strong adhesion). This consideration explains in particular the result of the experiment by DelRio *et al* [55] who observed that weak adhesion between Si and oxidized Si is due to the noncontact vdW interaction.

III. BEYOND THE COLUMNAR MODEL

It was established [78] that the shape of high peaks is described much better by a semispheroid than by a straight column or cone. We can improve the columnar model using this more realistic shape for high asperities. A high peak is described now by the upper half of a spheroid with the half-axes h_i (height, i enumerates the high peaks) and ξ (radius) as shown in Fig. 7. Deformations of such peaks can be described independently on each other because the average distance between them is large in comparison with the lateral size of asperities 2ξ.

As we already noted, the left-hand side of the balance equation (7) responsible for the attraction does not depend on the description of the peaks, which are not in direct contact with the flat plate. Only the repulsive force [right side of Eq. (7)] is sensitive to the shape of the peaks contacting with the flat plate. Since in equilibrium the pressure on all these peaks is the same and equal to P_f, the repulsive force is proportional to the relative area of real contact $R(h_0)$. However, beyond the columnar model this relative area does not reduced to the simple relation (5). In this section we are going to use more correct elastoplastic model and find the value of $R(h_0)$ for the case when the contacting peaks are described by semi-spheroids.

A. Deformation of a single peak

Let us start from the case of elastic deformations. As we know, in reality the elastoplastic contact is realized, but the elastic contact can be used to control the numerical calculations. The contact of a stiff flat plate with an elastic semi-spheroid can be described as the Hertzian contact [79] of a stiff plate and an elastic sphere of radius $\mathcal{R} = \xi^2/h_i$ with an effective Young modulus E^*. This effective modulus is a combination of the parameters of both interacting materials

$$\frac{1}{E^*} = \frac{1-\nu_1^2}{E_1} + \frac{1-\nu_2^2}{E_2}, \tag{13}$$

where $E_{1,2}$ and $\nu_{1,2}$ are the Young modulus and Poisson ratio of the materials. If the bodies are pressed together with the force F, the well-known results relate the force F and contact area S with the mutual approach δ [79]

$$F = \frac{4E^*}{3}(\mathcal{R}\delta^3)^{1/2}, \quad S = \pi\mathcal{R}\delta. \tag{14}$$

For the elastoplastic deformations one has to apply a force smaller than that given by Eq. (14) to produce the same approach, but the same δ will correspond to larger area of contact. To find the force and area of contact in the general case we have to do numerical simulations. The axisymmetric problem of elastoplastic compression of a semispheroid is solved by the method of finite elements (FEM). It is assumed that the semispheroid is a bump on an otherwise flat substrate of the same material. The semispheroid is compressed by a stiff flat plate.

Schematic presentation of the problem that is solved is shown in Fig. 7. The upper plate is assumed to be elastic with the Young modulus $E_2 = 160$ GPa and Poisson ratio $\nu_2 = 0.27$ (silicon). The lower plate is made of Au or Pt and assumed to be elastoplastic. The stress-strain dependence for gold was taken from the experimental data [73] for a nanocrystal with a size of 85 nm (closest to a grain size of 72 nm for Au film). The Young modulus determined from the same experiment is $E_1 = 60$ GPa and the flow stress we define as $P_f = 1.0$ GPa. For platinum the parameters have been taken from [76] where they have been determined from the molecular dynamics simulations. The case of Pt is nearly ideally elstoplastic with $E_1 = 121$ GPa and $P_f = 1.8$ GPa. The correlation lengths for both materials were taken from [48]. All the material parameters are collected in Table I.

TABLE I. Parameters used to calculate the deformation of a single elastoplastic semispheroid.

	ξ (nm)	E_1 (GPa)	ν_1	P_f (GPa)
Au	38	60	0.420	1
Pt	20	121	0.385	1.7
Si	flat	160	0.27	∞

The problem is solved in cylindrical coordinate system with consideration of finite deformations by use the FEM [80–82]. Only normal stresses are considered within the contact area. The bottom surface of the lower substrate as well as the top surface of the upper substrate are assumed to be rigid with ability to move in vertical direction only (Fig. 7). The process of the semispheroid deformation is simulated by a set of stationary contact problems being solved for a given mutual approach δ of the top and upper substrates which incrementally increased from 0 to some fixed value (3 nm).

The simulation results for pure elastic contact Si-Au are shown in Fig. 8 for $h_i = 14$ nm. One can see that both the force and area of contact as functions of the deformation reproduce well the Hetrtzian behavior for small deformations. Some deviations are observed for larger u since the relations (14) hold only for small deformations. Similar results have been found for Si-Pt elastic contact, which are shown in Fig. S1 [83].

Our main interest is in determination of the area of contact for the elastoplastic deformations. It has been calculated for four different values of height $h_i = 10, 12, 14, 16$ nm. For Si-Au contact the result is presented in Fig. 9 and for Si-Pt

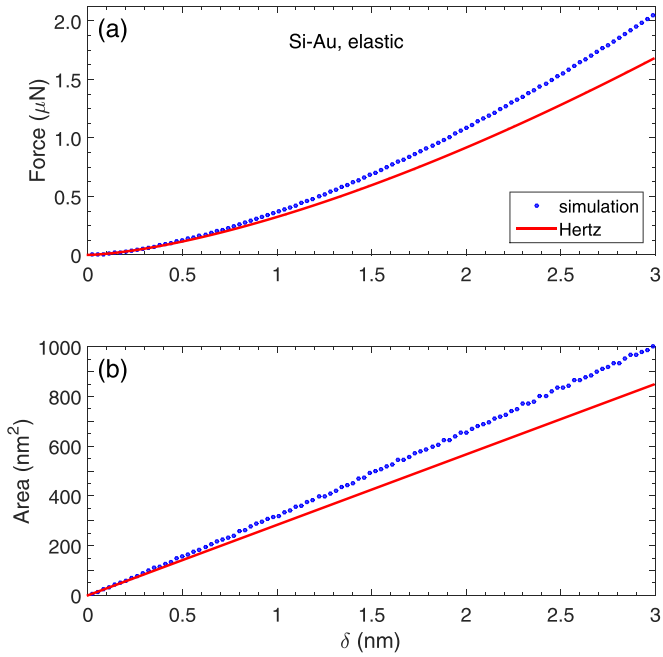

FIG. 8. Elastic contact Si-Au. (a) The force applied to the peak as a function of the approach δ. The result of simulation is shown by the blue dots. The red curve corresponds to the Hertz theory (14). (b) The area of contact as a function of the approach.

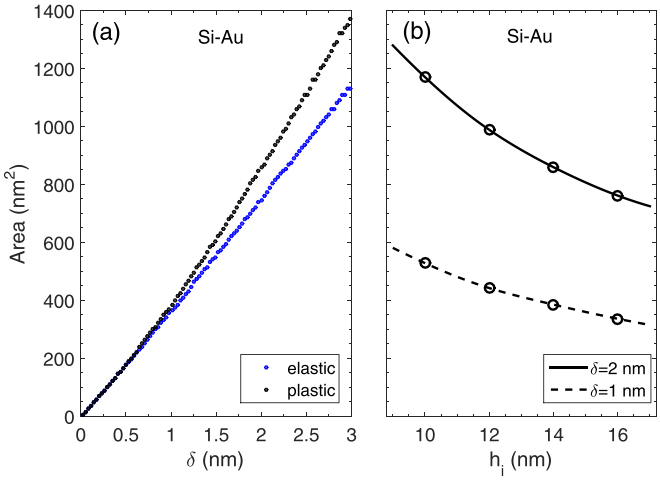

FIG. 9. Si-Au contact. (a) The area of contact as a function of the approach δ for the cases of elastoplastic (black dots) and pure elastic (blue dots) contacts. (b) The dependence of the contact area on the height of the peak for two values of δ. Open circles show the points of actual calculations connected by cubic interpolation.

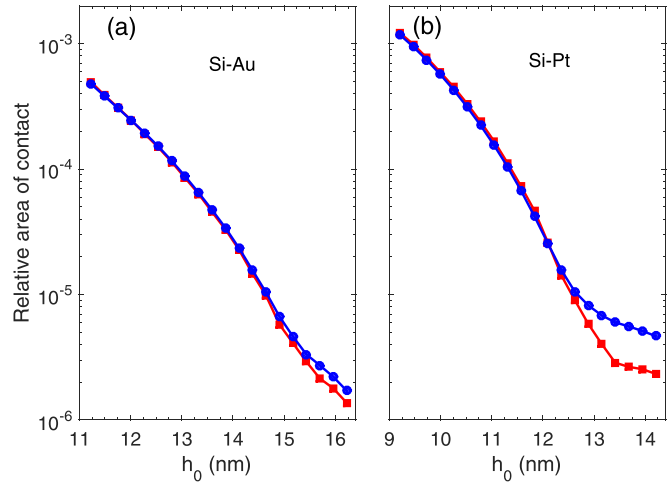

FIG. 10. (a) Relative area of contact for Si-Au system. Blue curve with circles (points of actual calculations) shows the result that has been found using the numerical calculations described in Sec. III A. For comparison the red curve with squares demonstrates the relative area for the simple columnar model. (b) The same for Si-Pt system.

contact the result is shown in Fig. S2 [83]. Figure 9(a) shows the area of elastoplasic contact (black dots) in comparison with pure elastic contact (blue dots) as a function of the approach. As one can expect the area of contact is larger for the elastoplastic case. On the other hand, the force that produces the same δ has to be larger for the elastic contact that is confirmed by Fig. S3 [83]. Figure 9(b) shows the area of contact as a function of the peak height h_i for two fixed values of δ. The actual calculations have been performed in the points indicated by the circles and the curves between these points were obtained by cubic interpolation. Similar results for Si-Pt contact are shown in Fig. S2 [83]. In comparison with the Si-Au case the area of contact for Si-Pt is significantly smaller that is explained by a considerably smaller grain size for Pt film.

B. Total area of contact

The area of contact for each peak depends on the initial height and lateral size. Using the AFM image of the rough plate we can find the heights h_i and radii ξ_i of the contacting asperities. All asperities with the height $h_i > h_{0p}$ are deformed elastoplastically. For ith peak the deformation generated by the short-distance repulsion will be $\delta_i = h_i - h_{0p}$. If we know the values for δ_i we can find the total area of contact or equivalently the relative area of contact $R(h_0)$ using the results of Sec. III A. Figure S4 [83] shows high-resolution binary images of Au and Pt films at the threshold height $z = 3w$ (0 for the pixels with $z < 3w$ and 1 for $z > 3w$). In panels (b) and (c) one can see those peaks that get into contact with the flat plate. Counting the number of bright pixels for each peak we can find the cross-section a_i of ith peak at the offset $z = 3w$ and assuming the spheroid shape it is possible to determine the individual radius ξ_i for each peak at the basement $z = 0$ using the relation

$$\xi_i = \sqrt{\frac{a_i}{\pi\left(1 - 9w^2/h_i^2\right)}}. \tag{15}$$

Averaging over all contacting asperities one can find the correlation length ξ_h for high peaks. For Au we have found $\xi_h = 35 \pm 3$ nm that agrees with the value $\xi = 38$ nm determined for all asperities. Similar for Pt we have found $\xi_h = 23 \pm 4$ nm (for all asperities $\xi = 20$ nm). It demonstrates that for high peaks the correlation length still keeps its meaning. However, it is more precise to use individual radii to calculate the area of contact since this area scales as ξ_i^2. Such a dependence suggested by the Hertz theory is supported by the numerical simulations.

The calculated area of contact for Si-Au and Si-Pt systems are shown in Figs. 10(a) and 10(b), respectively. These results can be compared with the simple columnar model, for which the relative area of contact is shown by the red curve. One can see that the columnar model reproduces well the more precise result, while a significant number ($\gtrsim$10) of high asperities takes part in the contact. If the contact is realized on a few asperities, then the columnar model underestimates the area of contact. It can be expected since the columnar model does not account for the area increase at plastic deformations. This effect becomes visible when the short-distance repulsion forces are distributed among few asperities. It is important to note that for both cases the equilibrium distances $h_0 = 14.8$ nm for Si-Au and $h_0 = 12.0$ nm for Si-Pt are in the range where the columnar model can be applied.

IV. DISCUSSION

The analysis presented in Sec. III shows that the simple columnar model adequately describes a realistic contact between rough and flat plates. On one hand, the attractive

interaction between plates is realized via the long-distance dispersion interaction. The rough surface is presented as a matrix of patches (AFM pixels) and the total attractive force is calculated as the sum over all patches separated from the flat plate by different local gaps. This approach is restricted only by the nonadditivity of DFs, but since we consider the distances smaller than the size of high asperities, nonadditivity is not an essential factor. On the other hand, the repulsive force that balances the attraction acts only in the places of direct contact between the plates. The high asperities contacting the flat plate are deformed plastically and AFM image data cannot be used to calculate the force. However, the numerical analysis demonstrated that these deformations do not change the area of contact significantly in comparison with the simple columnar model. Therefore, the columnar model can be used to evaluate both the attractive and repulsive forces.

The force balance equation (7) gives a way to evaluate the distance between the plates in contact (equilibrium distance h_0), if there is an AFM image of a sufficiently large area of the rough surface. This equation depends on the flow stress parameter P_f, which is defined by details of the material nanostructure. Due to uncertainty in P_f the equilibrium distance h_0 can vary. The decrease of P_f by half reduces h_0 by 0.8 nm for both gold and platinum films. It is not much better than the typical experimental precision in determination of h_0. The adhesion energy Γ is a direct consequence of the force balance as expresses Eq. (8), but the function $\Gamma(h_0)$ defined by this equation practically does not depend on P_f. Physically the Eqs. (7) and (8) carry the same information but both the force and energy can be measured independently.

Very weak dependence of Γ on the flow stress can be used to improve the precision of the force measurement in the distance range from 5 to 30 nm, where the force is difficult to measure with a decent precision due to pull-in instability and errors in determination of h_0. The pull-in instability can be overcome in the configuration of the adhered cantilever shown in Fig. 1. In this configuration the force can be measured as the deviation of the cantilever from a known classical shape. Simultaneously it is possible to measure the adhesion energy by measuring the unadhered length s. Here there are two possibilities.

First, if we know h_0, for example measured interferometrically, the value of Γ gives the magnitude of the dispersion interaction at the distance h_0, which is related to the force $P(h_0)$ by Eq. (9). In this case the information on the force extracted from the shape of the cantilever will be complimentary. This approach, however, does not allow reaching precision better than 30% at $h_0 \sim 10$ nm since the uncertainty in h_0 is about ± 1 nm.

Second, both values $P(h_0)$ and $\Gamma(h_0)$ have been measured at some unknown distance h_0. It is assumed that these values are defined by the dispersion interaction and we would like to compare them with the prediction of the Lifshitz theory. As was demonstrated in Sec. II D the function $\Gamma(h_0)$ practically does not depend on the parameters, which are not well known, including the flow stress or deformation of high asperities. Therefore, using the measured Γ we can find the value h_0 corresponding to this Γ in the Lifshitz theory. Even if Γ is measured with a modest precision, the corresponding value of h_0 will be known with precision better than ± 1 nm. For this h_0 we can then calculate the force $P_{\rm Lif}(h_0)$ and compare it with the measured value. This method gives a chance to improve the total precision in the force measurement at short distances.

V. CONCLUSIONS

In this paper we presented a full version of the Letter [21] where a relation between the adhesion energy and the distance upon contact has been deduced. We considered the contact of two rough plates with the aim to determine the equilibrium distance h_0 between them. Specificity of our problem is that the plates are contacting without an external load and nongaussian roughness of the plates with excessive number of high asperities is produced by typical deposition processes used in micro- and nanotechnologies. These conditions restricts the adhesion energies by rather small values $\Gamma \lesssim 100\ \mu\mathrm{J/m}^2$, which are usually not considered in the classical contact theory. This weak adhesion, however, is important for functioning of MEMS/NEMS devices and for precise measurement of the dispersion forces in the interval 5−30 nm.

The equilibrium between plates being in contact is established through balance of the attractive dispersion forces acting across the equilibrium gap h_0 and repulsive forces generated in the places of direct contact between high asperities and flat plate. This balance gives the equation (7) for determination of the distance h_0. The roughness of deposited films is characterized by a large number of high asperities, which are significantly higher than the rms roughness w. For this reason $h_0 \gg w$ and the adhesion is weak. The adhesion energy Γ given by Eq. (8) is determined via the forces acting between the plates.

The distance h_0 depends on plastic deformations of high asperities. The state of equilibrium is characterized by a fixed pressure on every asperity in contact. This pressure corresponds to the border separating plastic and elastic deformations and for metallic surfaces it can be identified with the flow stress P_f of the material. A specific nanostructure of the material results in uncertainty of this parameter, which propagates to uncertainty in the equilibrium distance. The most important conclusion is that in contrast with the value of h_0 the adhesion energy is practically not sensitive to the exact value of P_f. It means that the function $\Gamma(h_0)$ can be evaluated using only the Lifshitz theory, but the effects of contact interaction and plastic deformations in Γ can be neglected. We discussed the possibility to use this conclusion to improve determination of the equilibrium distance h_0 in the experiments where the force and adhesion energy are measured simultaneously.

ACKNOWLEDGMENT

This work is supported by the Russian Science Foundation, Grant No. 20-19-00214.

[1] H. B. G. Casimir, On the attraction between two perfectly conducting plates, Proc. Kon. Ned. Akad. Wetensch. **51**, 793 (1948).

[2] E. M. Lifshitz, The theory of molecular attractive forces between solids, Sov. Phys. JETP **2**, 73 (1956).

[3] I. E. Dzyaloshinskii, E. M. Lifshitz, and L. P. Pitaevskii, General theory of van der Waals' forces, Sov. Phys. Usp. **4**, 153 (1961).

[4] G. L. Klimchitskaya, U. Mohideen, and V. M. Mostepanenko, The Casimir force between real materials: Experiment and theory, Rev. Mod. Phys. **81**, 1827 (2009).

[5] A. W. Rodriguez, F. Capasso, and S. G. Johnson, The Casimir effect in microstructured geometries, Nat. Photonics **5**, 211 (2011).

[6] S. K. Lamoreaux, Demonstration of the Casimir Force in the 0.6 to 6μm Range, Phys. Rev. Lett. **78**, 5 (1997).

[7] B. W. Harris, F. Chen, and U. Mohideen, Precision measurement of the Casimir force using gold surfaces, Phys. Rev. A **62**, 052109 (2000).

[8] H. B. Chan, V. A. Aksyuk, R. N. Kleiman, D. J. Bishop, and F. Capasso, Quantum mechanical actuation of microelectromechanical systems by the Casimir force, Science **291**, 1941 (2001).

[9] R. S. Decca, D. López, E. Fischbach, and D. E. Krause, Measurement of the Casimir Force between Dissimilar Metals, Phys. Rev. Lett. **91**, 050402 (2003).

[10] R. Decca, D. López, E. Fischbach, G. Klimchitskaya, D. Krause, and V. Mostepanenko, Precise comparison of theory and new experiment for the Casimir force leads to stronger constraints on thermal quantum effects and long-range interactions, Ann. Phys. (NY) **318**, 37 (2005).

[11] D. Iannuzzi, M. Lisanti, and F. Capasso, Effect of hydrogen-switchable mirrors on the Casimir force, Proc. Natl. Acad. Sci. USA **101**, 4019 (2004).

[12] F. Chen, G. L. Klimchitskaya, V. M. Mostepanenko, and U. Mohideen, Demonstration of optically modulated dispersion forces, Opt. Express **15**, 4823 (2007).

[13] S. de Man, K. Heeck, R. J. Wijngaarden, and D. Iannuzzi, Halving the Casimir Force with Conductive Oxides, Phys. Rev. Lett. **103**, 040402 (2009).

[14] G. Torricelli, P. J. van Zwol, O. Shpak, C. Binns, G. Palasantzas, B. J. Kooi, V. B. Svetovoy, and M. Wuttig, Switching Casimir forces with phase-change materials, Phys. Rev. A **82**, 010101(R) (2010).

[15] G. Torricelli, P. J. van Zwol, O. Shpak, G. Palasantzas, V. B. Svetovoy, C. Binns, B. J. Kooi, P. Jost, and M. Wuttig, Casimir force contrast between amorphous and crystalline phases of AIST, Adv. Funct. Mater. **22**, 3729 (2012).

[16] P. J. van Zwol, G. Palasantzas, M. van de Schootbrugge, and J. T. M. De Hosson, Measurement of dispersive forces between evaporated metal surfaces in the range below 100nm, Appl. Phys. Lett. **92**, 054101 (2008).

[17] A. Tonck, F. Houze, L. Boyer, J. L. Loubet, and J. M. Georges, Electrical and mechanical contact between rough gold surfaces in air, J. Phys.: Condens. Matter **3**, 5195 (1991).

[18] M. Sedighi, V. B. Svetovoy, and G. Palasantzas, Casimir force measurements from silicon carbide surfaces, Phys. Rev. B **93**, 085434 (2016).

[19] V. B. Svetovoy, A. E. Melenev, M. V. Lokhanin, and G. Palasantzas, Global consequences of a local Casimir force: Adhered cantilever, Appl. Phys. Lett. **111**, 011603 (2017).

[20] V. B. Svetovoy, A. V. Postnikov, I. V. Uvarov, F. I. Stepanov, and G. Palasantzas, Measuring the Dispersion Forces Near the van der Waals–Casimir Transition, Phys. Rev. Applied **13**, 064057 (2020).

[21] I. A. Soldatenkov, G. Palasantzas, and V. B. Svetovoy, Weak adhesion between deposited rough films: Relation to the dispersion forces, Phys. Rev. B **104**, L121404 (2021).

[22] M. Sparnaay, Measurements of attractive forces between flat plates, Physica **24**, 751 (1958).

[23] G. Bressi, G. Carugno, R. Onofrio, and G. Ruoso, Measurement of the Casimir Force between Parallel Metallic Surfaces, Phys. Rev. Lett. **88**, 041804 (2002).

[24] J. Zou, Z. Marcet, A. Rodriguez, M. T. H. Reid, A. P. McCauley, I. I. Kravchenko, T. Lu, Y. Bao, S. G. Johnson, and H. B. Chan, Casimir forces on a silicon micromechanical chip, Nat. Commun. **4**, 1845 (2013).

[25] N. Tas, T. Sonnenberg, H. Jansen, R. Legtenberg, and M. Elwenspoek, Stiction in surface micromachining, J. Micromech. Microeng. **6**, 385 (1996).

[26] R. Maboudian and R. T. Howe, Critical review: Adhesion in surface micromechanical structures, J. Vacuum Sci. Technol. B **15**, 1 (1997).

[27] E. E. Parker, W. R. Ashurst, C. Carraro, and R. Maboudian, Adhesion characteristics of MEMS in microfluidic environments, J. Microelectromech. Syst. **14**, 947 (2005).

[28] E. Rabinowicz, *Friction and Wear of Materials* (Wiley, New York, 1995).

[29] F. M. Mwema, O. P. Oladijo, S. A. Akinlabi, and E. T. Akinlabi, Properties of physically deposited thin aluminium film coatings: A review, J. Alloys Compd. **747**, 306 (2018).

[30] B. N. J. Persson, *Sliding Friction: Physical Principles and Applications* (Springer, Heidelberg, 2000).

[31] J.-F. Zhao, A.-L. Wang, and C.-X. Yang, Prediction of thermal contact conductance based on the statistics of the roughness profile characteristics, Int. J. Heat Mass Transf. **48**, 974 (2005).

[32] B. Persson, B. Lorenz, and A. Volokitin, Heat transfer between elastic solids with randomly rough surfaces, Eur. Phys. J. E **31**, 3 (2010).

[33] S.-A. Biehs and J.-J. Greffet, Influence of roughness on near-field heat transfer between two plates, Phys. Rev. B **82**, 245410 (2010).

[34] B. N. J. Persson, Relation between Interfacial Separation and Load: A General Theory of Contact Mechanics, Phys. Rev. Lett. **99**, 125502 (2007).

[35] M. H. Müser, W. B. Dapp, R. Bugnicourt *et al.*, Meeting the contact-mechanics challenge, Tribol. Lett. **65**, 118 (2017).

[36] J. A. Greenwood and J. B. P. Williamson, Contact of nominally flat surfaces, Proc. R. Soc. A **295**, 300 (1966).

[37] K. N. G. Fuller and D. Tabor, The effect of surface roughness on the adhesion of elastic solids, Proc. R. Soc. A **345**, 327 (1975).

[38] J. F. Archard, Elastic deformation and the laws of friction, Proc. R. Soc. A **243**, 190 (1957).

[39] D. J. Whitehouse and J. F. Archard, The properties of random surfaces of significance in their contact, Proc. R. Soc. A **316**, 97 (1970).

[40] A. Bush, R. Gibson, and T. Thomas, The elastic contact of a rough surface, Wear **35**, 87 (1975).

[41] B. N. J. Persson, Theory of rubber friction and contact mechanics, J. Chem. Phys. **115**, 3840 (2001).

[42] B. N. J. Persson, Adhesion between Elastic Bodies with Randomly Rough Surfaces, Phys. Rev. Lett. **89**, 245502 (2002).

[43] B. Persson, Contact mechanics for randomly rough surfaces, Surf. Sci. Rep. **61**, 201 (2006).

[44] I. G. Goryacheva, *Contact Mechanics in Tribology* (Kluwer Academic Publ., Dordercht, 1998).

[45] T. Kim, B. Bhushan, and Y. Cho, The contact behavior of elastic/plastic non-Gaussian rough surfaces, Tribol. Lett. **22**, 1 (2006).

[46] G. Palasantzas, D. Tsamouras, and J. De Hosson, Roughening aspects of room temperature vapor deposited oligomer thin films onto Si substrates, Surf. Sci. **507-510**, 357 (2002).

[47] P. J. van Zwol, V. B. Svetovoy, and G. Palasantzas, Distance upon contact: Determination from roughness profile, Phys. Rev. B **80**, 235401 (2009).

[48] T. I. Muravyeva, I. V. Uvarov, V. V. Naumov, G. Palasantzas, and V. B. Svetovoy, Excessive number of high asperities for sputtered rough films, Phys. Rev. B **104**, 035415 (2021).

[49] P. J. van Zwol, G. Palasantzas, and J. T. M. De Hosson, Influence of random roughness on the Casimir force at small separations, Phys. Rev. B **77**, 075412 (2008).

[50] B. N. J. Persson and M. Scaraggi, Theory of adhesion: Role of surface roughness, J. Chem. Phys. **141**, 124701 (2014).

[51] J. A. Knapp and M. P. de Boer, Mechanics of microcantilever beams subject to combined electrostatic and adhesive forces, J. Microelectromech. Syst. **11**, 754 (2002).

[52] C. H. Mastrangelo and C. H. Hsu, Mechanical stability and adhesion of microstructures under capillary forces. I. Basic theory, J. Microelectromech. Syst. **2**, 33 (1993).

[53] C. H. Mastrangelo and C. H. Hsu, Mechanical stability and adhesion of microstructures under capillary forces. II. Experiments, J. Microelectromech. Syst. **2**, 44 (1993).

[54] M. P. de Boer and T. A. Michalske, Accurate method for determining adhesion of cantilever beams, J. Appl. Phys. **86**, 817 (1999).

[55] F. W. DelRio, M. P. de Boer, J. A. Knapp, E. D. Reedy, P. J. Clews, and M. L. Dunn, The role of van der Waals forces in adhesion of micromachined surfaces, Nat. Mater. **4**, 629 (2005).

[56] K. L. Johnson, K. Kendall, A. D. Roberts, and D. Tabor, Surface energy and the contact of elastic solids, Proc. R. Soc. A **324**, 301 (1971).

[57] B. Derjaguin, V. Muller, and Y. Toporov, Effect of contact deformations on the adhesion of particles, J. Colloid Interface Sci. **53**, 314 (1975).

[58] V. Muller, V. Yushchenko, and B. Derjaguin, On the influence of molecular forces on the deformation of an elastic sphere and its sticking to a rigid plane, J.Colloid Interface Sci. **77**, 91 (1980).

[59] J. Greenwood, Adhesion of small spheres, Philos. Mag. **89**, 945 (2009).

[60] P. Attard and J. L. Parker, Deformation and adhesion of elastic bodies in contact, Phys. Rev. A **46**, 7959 (1992).

[61] I. Soldatenkov, The use of the method of successive approximations to calculate an elastic contact in the presence of molecular adhesion, J. Appl. Math. Mech. **76**, 597 (2012).

[62] J. A. Greenwood and J. H. Tripp, The contact of two nominally flat rough surfaces, Proc. Inst. Mech. Eng. **185**, 625 (1970).

[63] J. N. Israelachvili, The calculation of van der Waals dispersion forces between macroscopic bodies, Proc. R. Soc. A **331**, 39 (1972).

[64] J. N. Israelachvili, *Intermolecular and Surface Forces* (Elsevier, Amsterdam, 2011).

[65] E. M. Lifshitz and L. P. Pitaevskii, *Statistical Physics, Part 2* (Pergamon, Oxford, 1980).

[66] E. D. Palik, ed., *Handbook of Optical Constants of Solids* (Academic Press, New York, 1985).

[67] V. B. Svetovoy, P. J. van Zwol, G. Palasantzas, and J. T. M. De Hosson, Optical properties of gold films and the Casimir force, Phys. Rev. B **77**, 035439 (2008).

[68] W. S. Choi, S. S. A. Seo, K. W. Kim, T. W. Noh, M. Y. Kim, and S. Shin, Dielectric constants of Ir, Ru, Pt, and IrO_2: Contributions from bound charges, Phys. Rev. B **74**, 205117 (2006).

[69] G. Munaò, A. Correa, A. Pizzirusso, and G. Milano, On the calculation of the potential of mean force between atomistic nanoparticles, Eur. Phys. J. E **41**, 38 (2018).

[70] J. Zhang, M. K. Borg, K. Sefiane, and J. M. Reese, Wetting and evaporation of salt-water nanodroplets: A molecular dynamics investigation, Phys. Rev. E **92**, 052403 (2015).

[71] E. N. Hahn and M. A. Meyers, Grain-size dependent mechanical behavior of nanocrystalline metals, Mater. Sci. Eng. A **646**, 101 (2015).

[72] J.-Y. Kim and J. R. Greer, Tensile and compressive behavior of gold and molybdenum single crystals at the nano-scale, Acta Mater. **57**, 5245 (2009).

[73] A. Sedlmayr, E. Bitzek, D. S. Gianola, G. Richter, R. Mönig, and O. Kraft, Existence of two twinning-mediated plastic deformation modes in au nanowhiskers, Acta Mater. **60**, 3985 (2012).

[74] J. Wang, F. Sansoz, J. Huang, Y. Liu, S. Sun, Z. Zhang, and S. X. Mao, Near-ideal theoretical strength in gold nanowires containing angstrom scale twins, Nat. Commun. **4**, 1742 (2012).

[75] A. A. Islam and R. J. Klassen, Kinetics of length-scale dependent plastic deformation of gold microspheres, J. Mater. Res. **32**, 3507 (2017).

[76] J. Li, B. Lu, H. Zhou, C. Tian, Y. Xian, G. Hu, and R. Xia, Molecular dynamics simulation of mechanical properties of nanocrystalline platinum: Grain-size and temperature effects, Phys. Lett. A **383**, 1922 (2019).

[77] X. W. Gu, C. N. Loynachan, Z. Wu, Y.-W. Zhang, D. J. Srolovitz, and J. R. Greer, Size-dependent deformation of nanocrystalline Pt nanopillars, Nano Lett. **12**, 6385 (2012).

[78] W. Broer, G. Palasantzas, J. Knoester, and V. B. Svetovoy, Roughness correction to the casimir force at short separations: Contact distance and extreme value statistics, Phys. Rev. B **85**, 155410 (2012).

[79] K. L. Johnson, *Contact Mechanics* (Cambridge University Press, Cambridge, 1985).

[80] L. Kogut and I. Etsion, Elasto-plastic contact of analysis of a sphere and a rigid flat, J. Appl. Mech. **69**, 657 (2002).

[81] R. L. Jackson and I. Green, A finite elements study of elasto-plastic hemispherical contact against a rigid flat, J. Tribol. **127**, 343 (2005).

[82] V. Brizmer, Y. Zait, Y. Klingerman, and I. Etsion, The effect of contact conditions and material properties on elastic-plastic spherical contact, J. Mech. Mater. Struct. **1**, 865 (2006).

[83] See Supplemental Material at http://link.aps.org/supplemental/10.1103/PhysRevB.105.075401 for Figures S1 through S4 and additional information on the numerical results is presented.